UNSTARTING PHENOMENA IN THE DESIGN OF A SUPERSONIC INLET TURBINE

*Noraiz Mushtaq and Paolo Gaetani**

Laboratory of Fluid Machines (LFM)
Department of Energy - Politecnico di Milano
Via Lambruschini 4, 20156 Milan, Italy
*Corresponding author: paolo.gaetani@polimi.it

ABSTRACT

A supersonic inlet turbine is an attractive solution to extract power from the highly fluctuating and supersonic flow delivered by a rotating detonation combustion chamber. To avoid unstarting in a supersonic inlet turbine, the best practice recommends maintaining the maximum contraction ratio above the self-started limit; nonetheless a complex unstarting mechanism was observed when a collective shock is generated. First, a thorough explanation is given on how a collective shock is formed ahead of the blade row and why this leads to the unstarting of a supersonic channel. Then, parametric analyses were carried out to evaluate the effect of Mach number, geometric and incidence angles on the collective shock unstarting limit. Finally, it is presented a comprehensive overview of all supersonic inlet turbine design limits, and design guidelines are updated in view of the further restrictions introduced by this additional constraint.

KEYWORDS

SUPERSONIC TURBINE, UNSTARTING, COLLECTIVE SHOCK, DESIGN LIMITS

NOMENCLATURE

A	Area $[m^2]$
Cp	Specific heat at constant pressure $[J\ kg^{-1}\ K^{-1}]$
g	Blade pitch $[m]$
H	Blade height $[m]$
i	Incidence angle [°]
$\dot{m}$	Mass flow rate $[kg\ s^{-1}]$
M	Mach number [-]
p	Pressure $[Pa]$
T	Temperature $[K]$
th	Leading-edge thickness $[m]$
U	Peripheral velocity $[m/s]$
V	Velocity $[m/s]$
α	Absolute flow angle with respect to axial direction [°]
α_g	Profile geometric angle [°]
β	Relative flow angle with respect to axial direction [°]
γ	Specfic heat ratio $[-]$
μ	Mach angle $[-]$
ρ	Density $[kg\ m^{-3}]$

Subscripts

1,2	Stator inlet and outlet, respectively
3,4	Rotor inlet and outlet, respectively
in	Inlet
n	Normal
ps	Post-shock
t	Total quantity
th	Throat
W	Relative frame of reference

Acronyms

CFD	Computational Fluid Dynamics
MOC	Method of Characteristics
RDC	Rotating Detonation Combustor
RDE	Rotating Detonation Engine

INTRODUCTION

Continuous growth in global energy consumption and climate change demand new solutions for clean and more efficient propulsion and power production devices. As for the land-based power systems, a substantial introduction of renewable technologies in the overall energy mix requires supporting energy systems to compensate for their intrinsic non-schedulability.

In this context, gas turbines still represent a viable option and one of the most promising solutions is their integration with rotating detonation combustors (RDC). In this technology, a detonation wave rotates typically in an annular chamber and burns the fresh mixture (Wolański 2013). The pressure gain originated from the detonation wave allows for a decrease in fuel consumption (Jones & Paxson 2013, Wintenberger & Shepherd 2006), an increase in total pressure (up to 15%) (Frolov et al. 2013), an increase of gas turbine thermal efficiency (Sousa, Paniagua & Collado Morata 2017, Strakey et al. 2016) and plant efficiency up to 14% over a conventional turbine (Claflin et al. 2014) for intermediate pressure ratios. Rotating detonation engine (RDE) are also perfectly compatible with hydrogen, owing to its aptitude to detonation (Anand & Gutmark 2019). Anand & Gutmark (2019) and Ma et al. (2020) have presented comprehensive reviews on the combustion issues.

The transonic/supersonic and highly fluctuating flow delivered by the combustor chamber is hardly suitable for the design of an efficient turbine. For this reason a diffusing transition duct for a subsonic turbine or an accelerating one for a supersonic turbine connects the combustion chamber to the first turbine stage (Braun et al. 2017, 2021). This paper focuses on the design issues of supersonic inlet turbines.

Supersonic inlet turbines are characterized by large work extraction at the expense of lower efficiencies compared to subsonic designs. Detailed analysis of the 3D design of supersonic turbines is carried out by Paniagua (Paniagua et al. 2014) and by Mushtaq et al. (Mushtaq, Colella & Gaetani 2022, Mushtaq, Persico & Gaetani 2022), where i) mean-line codes, ii) method of characteristics for the profile design, iii) high-fidelity CFD simulations, iv) shape optimization applied to endwalls, are combined to get a clear picture of the design complexity. Turbine interaction with the RDC was investigated numerically by Liu et al. (2019) and Shen et al. (2022) and experimentally by Bach et al. (2019).

Supersonic turbines for RDE applications have to comply with limitations characteristic of supersonic flows. Considering the unsteadiness of the incoming flow, the axial Mach number should be higher than sonic to avoid the unique incidence problem (Starken et al. 1984). Furthermore, the self-starting condition must be always satisfied since the normal shock wave of an un-started condition is considerably more dissipative than the bow-shock of a started condition. The self-starting condition constrains the maximum contraction ratio in the channel (Kantrowitz & Donaldson 1945), which in turn restricts the maximum allowable flow turning (Mushtaq, Colella & Gaetani 2022).

In this paper, unstarting phenomena are studied in detail by both analytical and CFD approaches. Results show that complex shock waves features at turbine inlet set an additional unstarting limit for supersonic inlet cascades. First, a detailed explanation is given on the mechanism behind this unstarting phenomenon. Then, parametric analyses reveal the effect of Mach number, geometric and incidence angle on this additional limit. Finally, supersonic inlet turbine constraints are compared in function of relevant design parameters to find the most severe limit for each configuration. From these analyses, some recommendations are provided for an efficient design of a supersonic inlet turbine.

DESCRIPTION OF THE UNSTARTING MECHANISM

The formation of a collective shock induces unstarting in a supersonic turbine. To fully understand this statement, it is first necessary to introduce the concept of collective shocks and then provide an explanation of how this phenomenon is responsible for the unstarting of a supersonic turbine.

A collective bow shock is formed when the bow shock waves generated by two close bodies merge together; it is critical to point that the coalescence of the two bow-shock waves happens only in certain conditions, which will be discussed in detail in the results section.
For example, Fig. 1 displays the schlieren images of an experimental campaign performed by Boiko in a shock tube (Boiko et al. 2004). As the distance between the two spherical bodies is reduced, three stages can be recognized: in the first one (a), each body generates a separate bow shock wave with a regular shock intersection; in the second stage (b), a Mach phenomenon is formed in the intersection point and finally, in the last one (c) the two shocks merge to generate a collective bow shock.

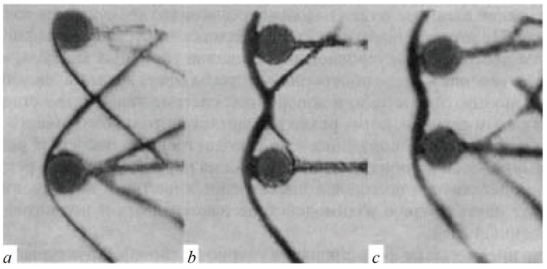

Figure 1: Schlieren photographs of the types of bow shock interference ahead of a transverse system of spheres (From Boiko et al. (2004)).

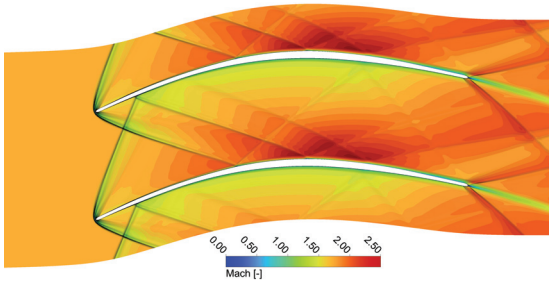

(a) Regular intersection

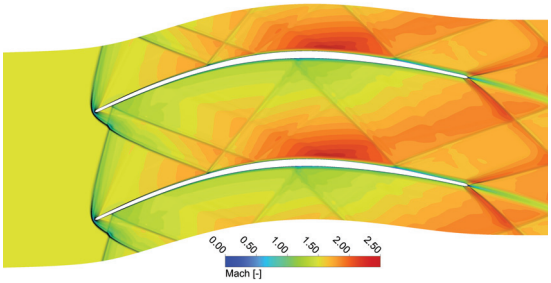

(b) Mach reflection

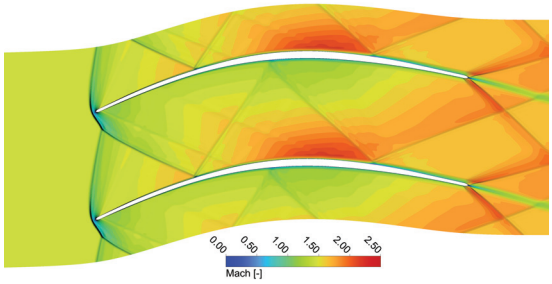

(c) Lambda shock

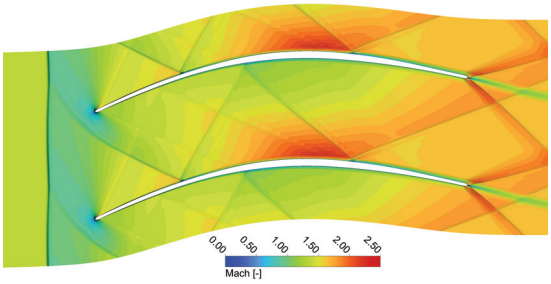

(d) Collective shock

Figure 2: Sequence of shock structures as the inlet Mach number is progressively reduced: there are respectively a regular intersection (a), a Mach reflection (b), a lambda shock (c) and finally a collective shock (d). The figures display in background the Mach field, while in foreground the shock structures are underlined by the density gradient. The inlet flow angle is aligned to the profile inlet geometric angle.

Since supersonic turbines generate bow shock waves at their leading edge, they are not exempt from the problem of collective shocks. In analogy to the Boiko campaign, if we progressively reduce the inlet Mach number while fixing the turbine geometry, the bow shock waves widen manifesting a series of distinct shock structures (Fig. 2): these include a regular intersection (a), a Mach reflection (b), a lambda shock (c) and finally a collective shock (d) in order of appearance at decreasing inlet Mach numbers. Overall, the formation of these structures is a complex phenomenon, that depends on various factors such as the geometry of the turbine and the incoming flow. Downstream of a strong collective shock the flow can still become supersonic in the turbine channel as displayed by case (d), where the area contraction induced by the leading edge is responsible for the supersonic transition (the post-shock Mach number was close to unity).

However, the collective shock for a supersonic turbine presents some distinct features. First of all, due to the periodicity of the turbine, the collective shock is almost a straight shock without the bowed end in the external region (Fig. 1). Furthermore, collective shock have been primarily studied for external aerodynamics (Laurence et al. 2007), while in this case the collective shock is formed inside a supersonic channel, which is already affected by starting/unstarting issues. Considering the flow orientation, which is not necessarily aligned to the channel axis, the collective shock behaves as an oblique shock wave (Fig. 3). As the flow goes through the oblique collective shock, the flow is turned in tangential direction by an angle θ, which can be interpreted as a reduction of the effective area. The contraction ratio for a turbine channel is calculated in Eq. 1 and simplified for a constant channel geometry; in addition, numerical examples are reported in table 1 for the contraction ratios caused by collective shocks. Unfortunately, a shock wave is unstable in a converging duct: the collective shock starts moving upstream in search for a stable position leading ultimately to the unstarting of the supersonic channel.

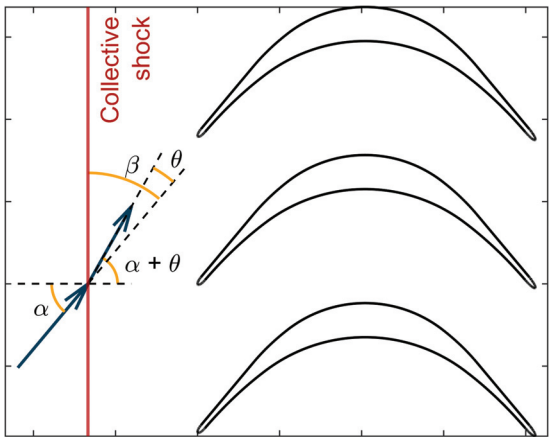

Figure 3: Flow turning induced by the collective shock, which behaves as an oblique shock wave ahead of the blade row.

$$\frac{A_{ps}}{A_1} = \frac{2\pi r_{ps} H_{ps} cos\left(\alpha_{ps}\right)}{2\pi r_1 H_1 cos\left(\alpha_1\right)} = \frac{cos\left(\alpha_{ps}\right)}{cos\left(\alpha_1\right)} \tag{1}$$

Collective shock unstarting is also characterized by an upper limit, because for certain conditions (high inlet geometric angles and low inlet Mach numbers) the bow shock waves are so

Table 1: Contraction ratios caused by the collective shock (oblique shock).

M_1	α_1	α_{ps} (post shock)	A_{ps}/A_1
1.4	25°	34.3°	0.911
1.7	40°	51.9°	0.805
2	50°	60.6°	0.763

wide that there is no intersection between them. This upper limit is estimated in Eq. 2 assuming that detached waves are asymptotic to the free-stream Mach lines at large distances from the leading edge (Moeckel 1921). One unexpected outcome is that collective shock unstarting and unique incidence problem are mutually exclusive, since the first one requires a supersonic axial Mach number, while the second one a subsonic axial Mach number (Eq. 3).

$$\begin{cases} sin\mu = \dfrac{1}{M_{in}} & \text{Mach angle} \\ \mu > 90° - \alpha_g & \text{Condition for no intersection} \end{cases} \tag{2}$$

$$M_{in}cos(\alpha_g) = M_{in-axial} < 1 \tag{3}$$

Collective shock unstarting and the well-known Kantrowitz limit may seem very similar at first glance, but there are relevant differences between the two phenomena. The Kantrowitz limit (Kantrowitz & Donaldson 1945) provides the maximum allowable contraction ratio (Eq. 4) for a diffuser to ingest the normal shock generated during the starting process and obtain a supersonic flow; once the supersonic diffuser is started, the contraction ratio necessary for the unstarting is significantly smaller and corresponds to a sonic condition in the throat. The hysteresis of the Kantrowitz limit is clearly displayed in Fig. 4 by the starting and unstarting arrows.

$$\begin{cases} \left.\dfrac{A_{th}}{A_{in}}\right|_{self-started} > \left(\dfrac{\frac{\gamma+1}{2}}{1+\frac{\gamma-1}{2}M_n^2}\right)^{\frac{\gamma+1}{2(\gamma-1)}} \\ \\ M_n^2 = \dfrac{(\gamma-1)M_{in}^2+2}{2\gamma M_{in}^2-(\gamma-1)} \end{cases} \tag{4}$$

On the contrary, no hysteretic behavior was observed in this novel mechanism for supersonic turbine unstarting, because the formation of a collective shock depends only on the bow shock waves; the bow shock shape and their intersection is determined by turbine inlet conditions and not on the previous states. It is relevant to underline that in this consideration, turbine inlet conditions are varied slowly enough to establish a quasi-steady flow in the turbine, while the effect of upstream unsteadiness on collective shock unstarting will be examined in detail in a subsequent work.

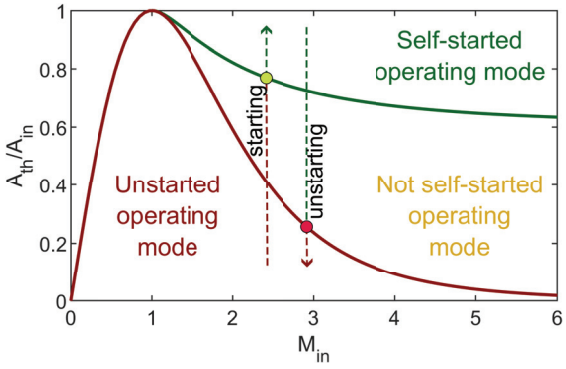

Figure 4: Contraction ratio allowed by the Kantrowitz limit at varying inlet Mach number. The hysteresis between the starting and unstarting condition is highlighted by upward and downward arrows, respectively.

METHODS

Computational flow model

Ansys CFX was selected to perform the quasi 2D blade-to-blade CFD simulations. The pressure-based implicit coupled solver has been validated for supersonic flows against two test cases (Fig. 5): the analytical solution of the Sod shock tube (Sod 1977) and the experimental data on a 2D compression corner (Settles & Dodson 1991). The advection terms were modelled with high-resolution schemes implemented as a total variation diminishing algorithm (Druguet & Zeitoun 2003), while the transient terms were discretized with a second order backward Euler scheme. Viscous calculations are necessary to accurately simulate cases characterized by boundary layer separation due to large incidence angles; turbulence closure was achieved through the k-omega SST model and y^+ was kept below 1 on all wall surfaces. The working fluid is air which is assumed to be a perfect gas.

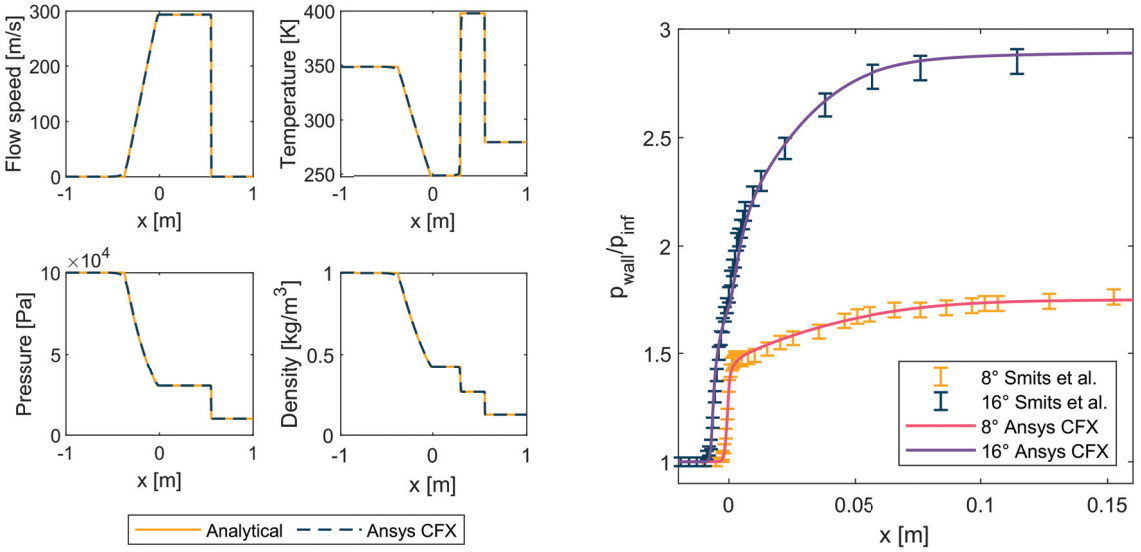

(a) **(b)**

Figure 5: (a) Comparison between the analytical and Ansys CFX solution at t = 0.001 s for the Sod shock tube problem. (b) Comparison between the experimental solution and Ansys CFX for the compression corner problem at 8°and 16°ramp angles.

Pressure, temperature and velocity are all assigned at the supersonic inlet. The blade profile is an adiabatic and no-slip boundary, while adiabatic and free-slip conditions are prescribed on the hub and shroud walls. The outlet is supersonic and the lateral boundaries are periodic. Computations were considered at convergence when at each time step (or at the last step for a steady-state simulation) all the residuals were below $5 \cdot 10^6$.

Ansys TurboGrid was used to generate a structured mesh with hexahedral cells, high orthogonality, and low skewness. The domain was modelled as a periodic annular stream tube (small thickness in radial direction) placed at a large radius to minimize curvature and radial equilibrium effects; this strategy was necessary since the meshing software, which produces excellent quality mesh for turbines, works in cylindrical coordinates and with three-dimensional domains. The inlet is situated one chord upstream of the leading-edge to capture the collective shock, while the outlet is located half-chord downstream of the trailing-edge. The mesh independence analysis was carried out with the grid convergence index method (Celik et al.

2008). For the blade-to-blade simulations (2 cells in radial direction), 100 k, 200 k, 400 k and 800 k were tested. The 400k satisfied the independence condition: the grid convergence index from fine to medium mesh calculated on the mixed-out entropy production (Prasad 2004) is 0.59%. Complete details about the case set-up and the solver validation are reported in (Mushtaq, Colella & Gaetani 2022).

Automated procedure for unstarting limit detection

Parametric analyses are necessary to evaluate the effect of this complex unstarting mechanism on the design space available for a supersonic turbine. Since unsteady simulations have a prohibitive computational cost for extended parametric analyses, a procedure based on steady-state simulations was developed to find the unstarting limit curve.

In this procedure, consecutive steady-state simulations are performed where only one parameter is modified, while all the others are maintained constant. As an example, let's consider that, for a given geometry and flow angle, we want to determine the limit Mach number for un-starting. The initial point is a Mach number sufficiently high that the supersonic profile is in a started operating mode. After each steady-state simulation, the inlet Mach number is reduced of ΔM with respect to the previous one, and the solution of the previous simulation is used as initial condition to further reduce the computational cost. The process continues till a collective shock is formed ahead of the blade row and starts moving upstream in the time-marching steady state solver. The procedure is finally repeated for different geometric and incidence angles to build the parametric unstarting limit curves.

The geometry of the turbine is generated without aiming to the maximum performance, but to isolate unstarting by collective shock from the other limits of a supersonic turbine; hence, the outlet flow angle, the leading-edge thickness to pitch ratio and the stream-tube channel height ratio have been selected to avoid Kantrowitz type unstarting in all cases. The supersonic profiles are generated with the "vortex-flow" method, which is an implicit Method Of Characteristics (MOC) developed by Goldman & Vanco (1971). Since the MOC generated profile has infinitesimal thickness at the leading and trailing edge, the pressure side and suction side are shifted of a plausible thickness value and closed by ellipses.

The procedure based on steady-state simulations was validated with an unsteady simulation. In the unsteady simulation, the inlet Mach number was modified in time with a stepwise trend: the Mach number is reduced in each step by ΔM and then sufficiently time is conceded to reach a steady solution or to manifest the unstarting phenomenon. The ΔM selected for both methodologies is equal to 0.025, which is a reasonable compromise between accuracy and computational cost. A value of 25° was selected for the inlet flow angle, the outlet flow angle is half of the inlet flow angle, the stream-tube channel height ratio is 1.2 and the pitch to leading-edge thickness ratio is 42. Inlet flow direction (25°), static pressure (1.92 bar) and static temperature (1300 K) were maintained constant. The starting Mach number obtained with the steady and unsteady simulations are respectively 1.361 ± 0.025 and 1.375 ± 0.025. Since the two values are within ΔM, the procedure based on steady-state simulations can be reliably employed to generate the parametric curves for the unstarting limit.

RESULTS AND DISCUSSION

The effect of Mach number, geometric and incidence angles on the unstarting limit

The effect on the starting limit of the inlet Mach number, the profile inlet geometric angle α_g and the incidence angle i was investigated, since these quantities are extremely relevant both

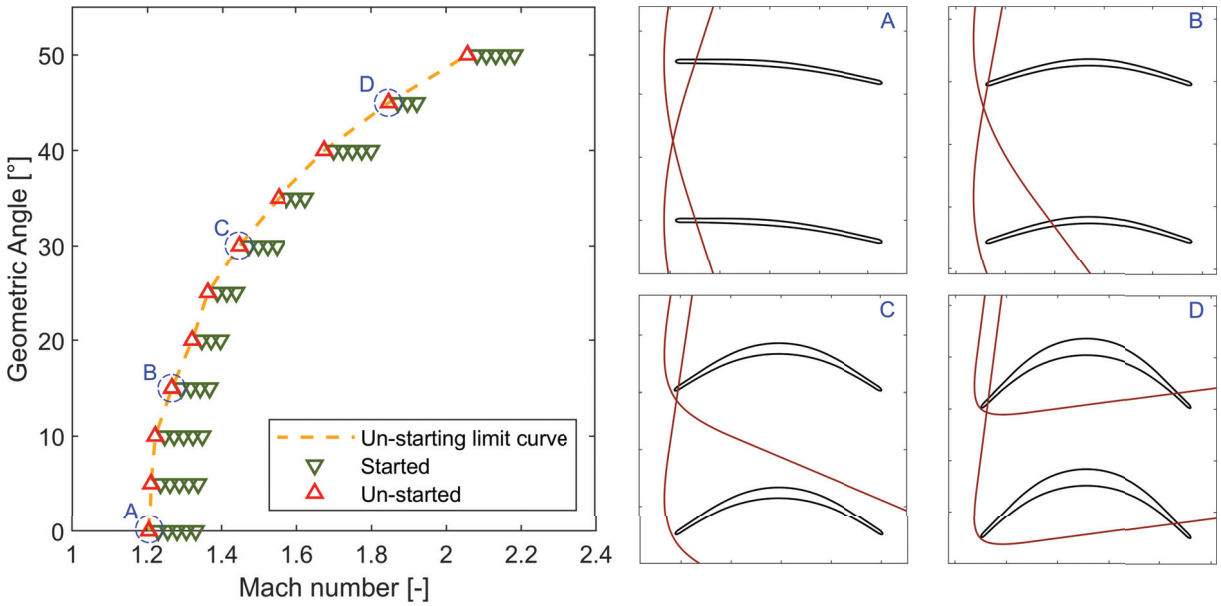

Figure 6: Maximum inlet geometric angle for collective shock unstarting at varying inlet Mach number. Green and red triangles are associated to a started and unstarted turbine operation, respectively. A, B, C and D are sketches of the bow-shock waves associated to the operation points circled in the left figure.

for the turbine design and its integration with a rotating detonation combustor. About 200 CFD simulations were carried out to build the parametric curves displayed in the next pages with the procedure presented and validated in the methods section. Turbine inlet conditions were selected considering typical values for RDEs and high-pressure turbines (Schwer & Kailasanath 2010, Paniagua et al. 2014, Paxson & Naples 2017, Rankin et al. 2017, Braun et al. 2021); notice that the velocity intensity and direction were varied, while the static pressure (1.92 bar) and static temperature (1300 K) were maintained constant throughout the procedure.

Figure 6 displays the unstarting limit curve that relates the inlet Mach number and the inlet geometric angle. The points marked with the green and red triangles correspond respectively to started and un-started blade rows, assessed by means of CFD simulations. This curve reveals that higher inlet geometric angles demand higher inlet Mach numbers to avoid unstarting by collective shock.

To understand this trend, it is important to remember that a collective shock is generated by the coalescence of the bow shock waves, which takes place only in certain conditions. The geometric angle does not affect the shape of the shock, but it modifies the location of the intersection point. For higher geometric angles, the intersection point shifts from the center of the channel towards one of the leading edges and closer to the normal portion of the bow shock wave. Under these conditions, the bow-shock waves undergo partial merging manifesting a characteristic Mach reflection structure, composed of a normal shock between the two triple points (Délery & Dussauge 2009). If the inlet geometric angle were to be further increased, it would lead to a complete merger of the shock waves anticipating the formation of a collective shock. Hence, high inlet geometric angles require high inlet Mach numbers to reduce the slope of the bow shock waves leading to more regular intersections. For low geometric angles, the shock intersection is closer to the center of the channel, which enables the starting of the turbine even with

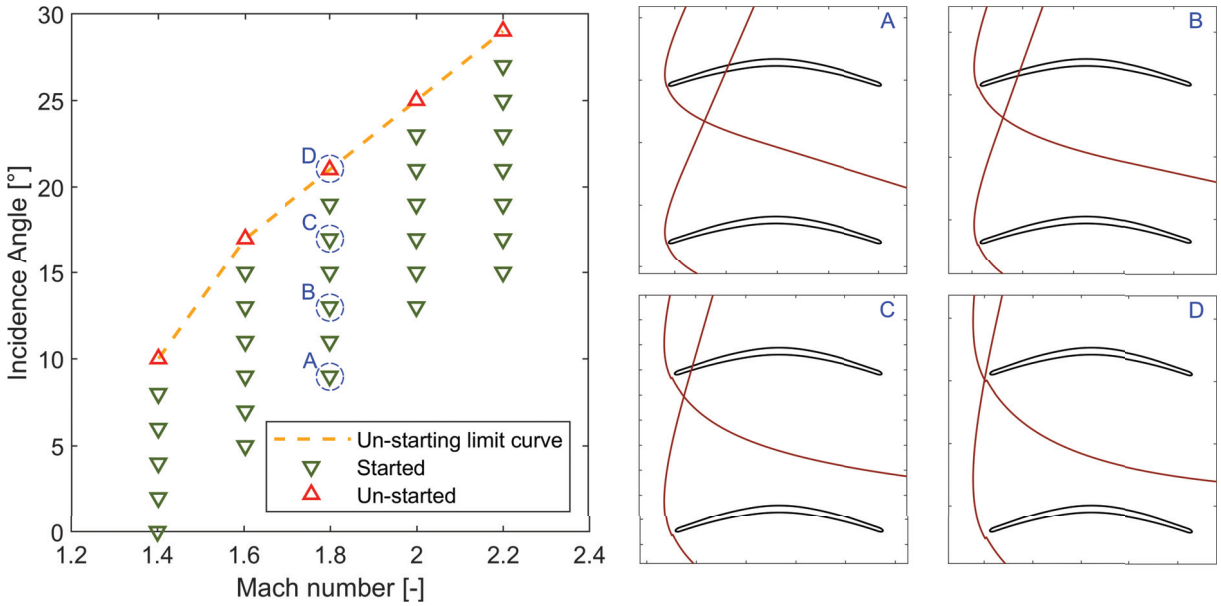

Figure 7: Maximum incidence angle for collective shock unstarting at varying inlet Mach number and for an inlet geometric angle of 15°. A, B, C and D are sketches of the bow-shock waves associated to the operation points circled in the left figure.

wider bow shock waves produced by lower inlet Mach numbers.

Assessing the influence of the incidence angle on the starting limit is valuable considering typical RDE off-design operations and highly fluctuating flows at turbine inlet ($\pm 20°$). By way of example, the relationship between the Mach number and the incidence angle for a fixed geometric angle of 15° is shown in Fig. 7; in this case, the Mach number was maintained constant, while the incidence angle was progressively increased until the appearance of the unstarting phenomenon. When the flow is not aligned with the profile (non-zero incidence angle), an asymmetrical bow shock wave is generated at the blade leading edge; as the incidence angle is increased, one of the branches of the shock wave rapidly moves upstream facilitating the formation of the collective shock. This issue can be mitigated by less inclined bow shock waves, which explains why higher inlet Mach numbers can accept larger incidence angles.

Furthermore, figure 8 underlines the detrimental effect of the geometric angle α_g on the Mach-incidence relation. As explained earlier, an increase in the geometric angle has no effect on the bow-shock shape, but it shifts the intersection point towards un unfavorable location from the starting point of view. It is also relevant to observe that the effect of the geometric angle is non-linear; the variation in geometric angle between the three curves is the same, but the shift for the 30° geometric angle is considerably larger than the 15° one. This characteristic originates from the Mach - α_g relation (Fig. 6): the impact of the geometric angle on the Mach number is limited below 15°, which explains the reduced shift between the 0° and 15° geometric angle curves.

In conclusion, these parametric curves further demonstrate the pivotal role of the shock structures in the unstarting by collective shock, where the adverse effects of an increase of the geometric angle and incidence angle are counterbalanced only by an increase of the Mach number.

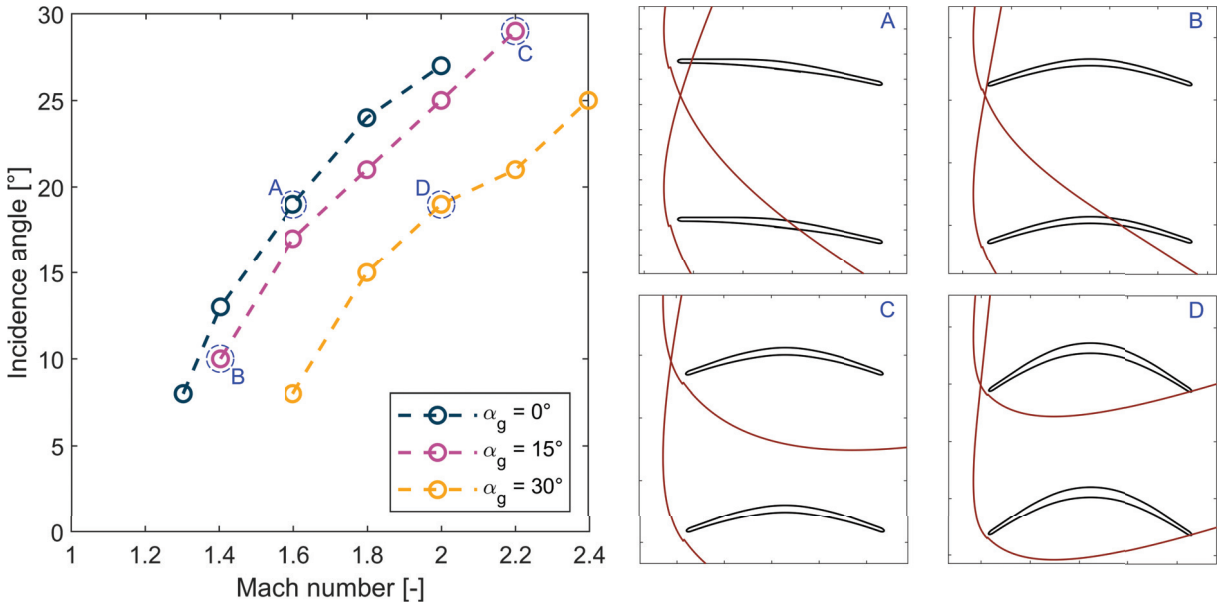

Figure 8: Influence of the geometric angle on the maximum incidence angle for collective shock unstarting. A, B, C and D are sketches of the bow-shock waves associated to the operation points circled in the left figure.

Design limits for supersonic inlet turbines

Once the mechanism behind collective shock unstarting has been understood and the effect of the inlet quantities investigated, it is appropriate to compare this additional limit with the known ones and determine if and how guidelines change for the design of a supersonic inlet turbine. First, an overview of all the limits in the design of a supersonic stator-rotor configuration is presented in Fig. 9.

Three limits constrain stator inlet geometry: 1) the Kantrowitz limit on the area contraction caused by the leading-edge thickness, 2) the collective shock unstarting and 3) the unique incidence problem. Among these, the restriction on the pitch to leading edge thickness ratio g/th (Fig. 9b) represents a far limit because the value of this ratio is typically higher than the limit value to minimize bow-shock losses. The unique incidence problem should also be avoided since large fluctuations are still expected at stator inlet ($\pm$ 20°).

Kantrowitz limit also restricts stator outlet flow angle and the design space can be extended with a variable stator blade height because the area reduction caused by larger flow angles is compensated by an increase in blade height at the outlet (Mushtaq, Colella & Gaetani 2022, Sousa, Paniagua & Saavedra 2017). Notice that the limitation on stator outlet flow angle is more severe than stator inlet limits and demands for higher inlet Mach numbers; this option further improves safety margins on stator inlet limits.

On the contrary, rotor inlet constraints are severe and their requirements grave on the turbine design and performance. These are the same limits described for the stator, just in the relative frame of reference; the main issue is that a lower rotor inlet Mach number (diffusing stator channel) minimizes shock losses, but it also increases the severity of rotor inlet limits.

Efficient supersonic inlet turbines are characterized by large stator outlet flow angles with minimum rotor inlet shock losses (Mushtaq, Persico & Gaetani 2022). Unfortunately, the optimum efficiency direction is moderated by stator outlet and rotor inlet constrains. Therefore, to

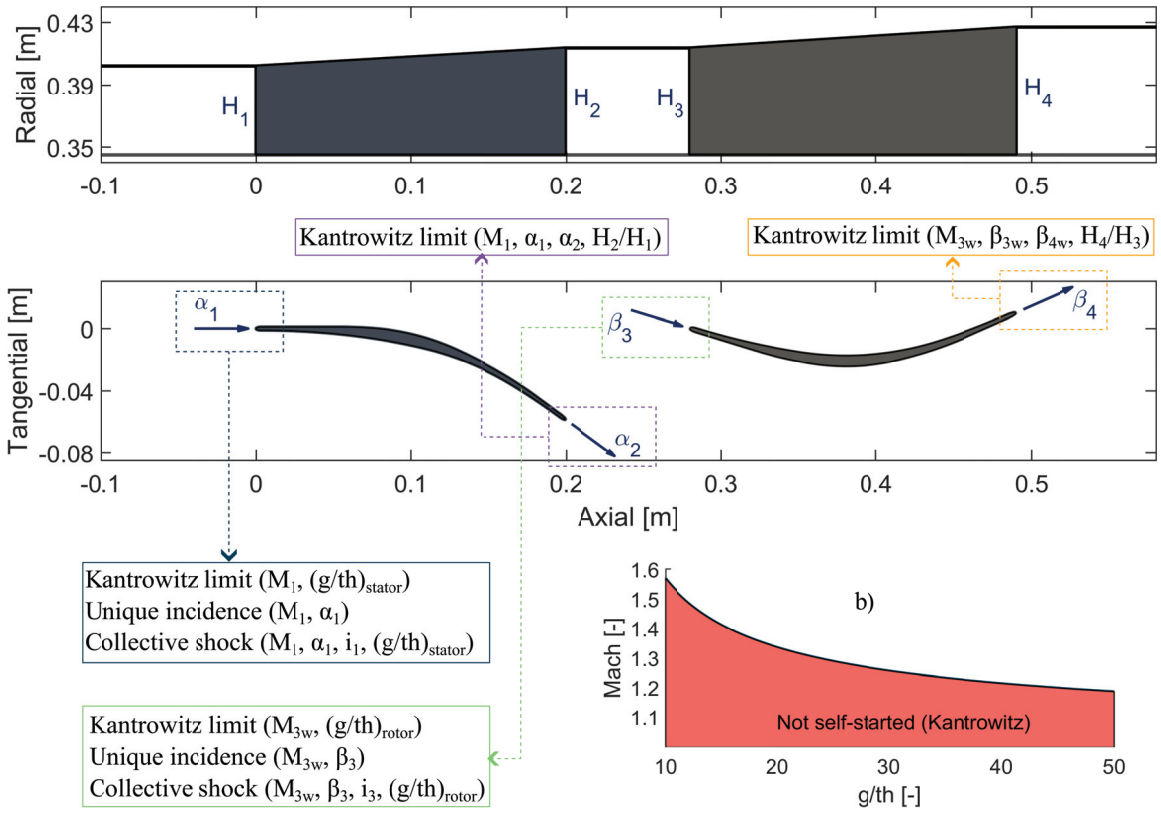

Figure 9: a) Overview of all the constraints in the design of a supersonic inlet turbine. For each constraint, the main dependencies are listed within the brackets. b) Minimum pitch to leading edge thickness to avoid unstarting by Kantrowitz at turbine inlet.

find the optimum compromise it is essential to understand the trend of these limits in function of relevant design parameters.

For this purpose, it was employed an in-house mean-line code specifically developed and validated for the design of supersonic inlet turbines for RDEs (Mushtaq, Colella & Gaetani 2022, Mushtaq, Persico & Gaetani 2022).

Aerodynamic losses were estimated to correctly predict rotor inlet flow quantities and consequently rotor inlet limits. An accurate evaluation of stator entropy production was achieved by taking into account: 1) the leading-edge bow shock wave losses, estimated thanks to the methodology developed by Moeckel to predict bow-shock wave shape for two dimensional or axial symmetric bodies (Moeckel 1921, Klapproth 1950); 2) boundary and mixing losses obtained by first calculating the compressible turbulent boundary layer quantities using Stratford and Beavers procedure (Stratford & Beavers 1961) and then the overall loss coefficient is evaluated by extending Stewart's method for supersonic axial Mach numbers (Stewart 1955); 3) endwall losses determined by integrating Coull's equation (Coull 2017) with Truckenbodt's correlation (Moore & Moore 1983) for the dissipation coefficient.

The variables selected for the parametric analysis are stator inlet Mach number M_1, stator outlet flow angle α_2 and stator outlet/inlet blade height ratio H_2/H_1. Rotor peripheral velocity was maintained constant because its effect on collective shock unstarting is negligible; this result comes from the fact that a reduction in relative flow angle at higher peripheral velocity is balanced by a reduction in relative inlet Mach number. The dimensionless ratios (pitch to leading

edge thickness ratio, solidity and blade aspect ratio) have been carefully selected considering the thermal and the mechanical integrity of the profiles (further details are provided in (Mushtaq, Persico & Gaetani 2022)). Table 2 reports the inlet flow quantities that were kept fixed during the parametric analysis.

The limit value for each constraint was found through a binary search algorithm (Knuth 1997); for a given couple $(M_1, H_2/H_1)$, the maximum stator outlet flow angle was determined by progressively halving the search interval, where the lower and upper limit of the interval does and does not respect the limit, respectively. The process was considered at convergence when the interval length was below 0.1°. The same procedure was then repeated for each limit and for various Mach numbers and stator blade height ratios.

Table 2: Constant input parameters for the parametric analyses.

Mass flow rate [kg/s]	100
Total Pressure [bar]	15
Total Temperature [K]	2150
Peripheral speed [m/s]	400
α_1 [deg]	0

At last, there is still one trivial but fundamental condition to satisfy: mass conservation. In a supersonic turbine, mass flow rate is assigned by the inlet flow conditions and must be obviously conserved in the stator and rotor blades.

$$\dot{m} = \rho_2 A_{2n} V_2 = \frac{p_{2t}}{\sqrt{Cp\, T_{2t}}} A_{2n} \frac{\gamma}{\sqrt{\gamma - 1}} \left(1 + \frac{\gamma - 1}{2} M_2^2\right)^{-\frac{\gamma+1}{2(\gamma-1)}} M_2 \tag{5}$$

Equation 5 clarifies the relation between mass flow rate, total quantities and Mach number; by way of example, this relation is displayed in Fig. 10 for various total pressures and stator outlet flow angles. It is interesting to observe that lower total pressures and larger outlet flow angles shift the curve towards lower values of the mass-flow rate. This condition arises also for supersonic turbines when extremely high values of the outlet flow angles are considered with significant total pressure losses in the stator blade row. In this situation, no stator outlet Mach number is able to transport the mass flow rate assigned at inlet making the corresponding geometry inadmissible.

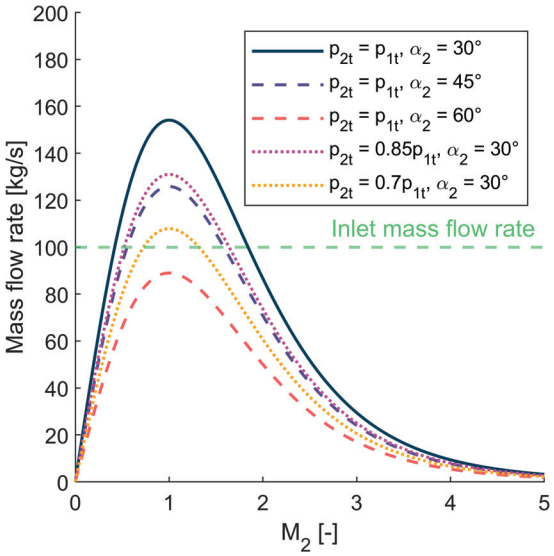

Figure 10: Mass flow rate at stator outlet for various total pressures and outlet flow angles.

The maximum stator outlet flow angle with a constant stator blade height accepted by the most severe stator outlet and rotor inlet constraints is displayed in Fig. 11a. It is critical to observe how collective shock unstarting is the prevailing limit for almost all Mach numbers and neglecting this additional unstarting mechanism during the design stage may have grave consequences on the turbine and engine operations. For increasing stator inlet Mach numbers (and hence M_{3W}), the Kantrowitz limit on the stator becomes the ruling constraint since collective shock limit rapidly mitigates for higher values of M_{3W}. The unique incidence limit and the collective shock one present similar trends because they both depend on the same variables (Fig. 11a) for

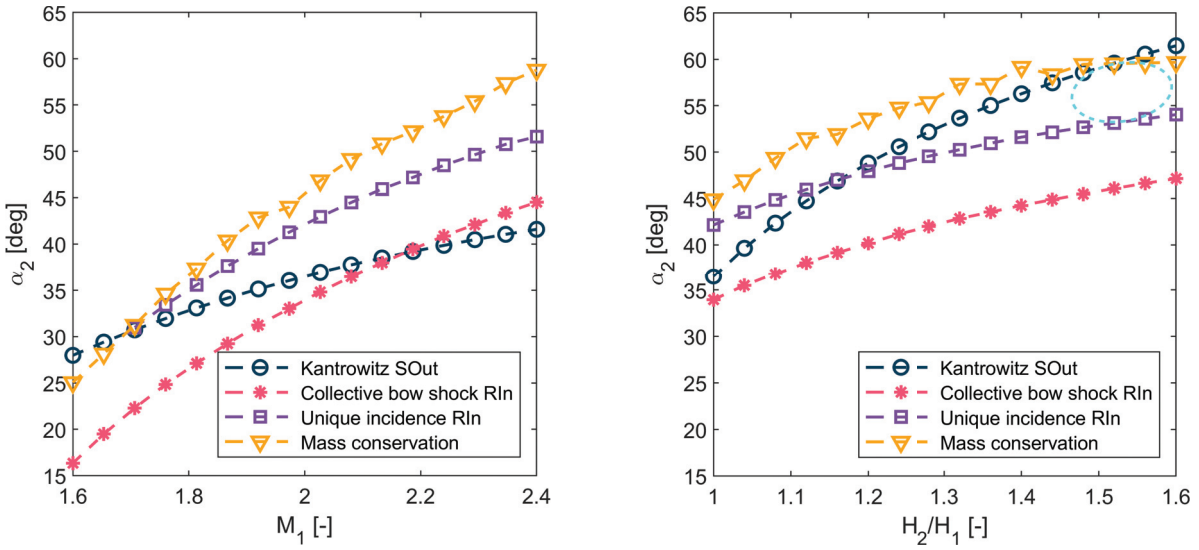

Figure 11: Maximum stator outlet flow angle allowed by stator outlet (SOut) and rotor inlet (RIn) constraints with a stator blade height ratio of 1 (a) and with an inlet Mach number of 2 (b). For both cases, zero incidence angle was considered at rotor inlet. The circled area in (b) highlights a high flow-turning region which suffers only from the unique incidence problem.

constant values of rotor incidence angle and rotor g/th ratio. Finally, mass conservation typically provides a far limit, which cannot be reached due to the restrictions imposed by the other constraints.

Furthermore, the relation for each limit between the maximum stator outlet flow angle and stator blade height ratio H_2/H_1 is presented in Fig. 11b. Kantrowitz limit exhibits a strong dependency on H_2/H_1 ratio because, as stated earlier, contraction of the blade-to-blade channel can be mitigated by expanding the blade height. Additionally, higher values of H_2/H_1 increases stator outlet Mach number and hence rotor inlet M_{3W}; thus, the maximum α_2 allowed by the collective shock unstarting is also larger. It is worth noting that the rate of increase in stator outlet flow angle is slower for the collective shock compared to the Kantrowitz limit. This is because the additional blade height ratio cannot be fully converted into flow angle without risking collective shock unstarting.

Figure 11 a and b provide valuable information for the design of the supersonic turbine and for the design of the transition duct. At lower stator inlet Mach numbers, flow turning is significantly limited with reduced work generation; on the contrary, larger flow angles are possible with higher inlet Mach numbers, but stator shock losses will increase accordingly. Therefore, the choice of the inlet Mach number is mainly driven by the required work specification.
Variable stator blade height is still a beneficial option to improve turbine efficiency by producing a large amount of work with limited variation in losses (Mushtaq, Persico & Gaetani 2022). The main difference is that the maximum stator outlet flow angle is driven by collective shock unstarting and not by the Kantrowitz limit.
Furthermore, Fig. 11b reveals an alternative solution: at high H_2/H_1 ratios, there is an area that suffers from unique incidence problem, but it is below the Kantrowitz limit (collective shock unstarting is not possible above the unique incidence line). A designer can decide to work in

this area (circled in Fig. 11b) accepting the unique incidence problem, an approach already employed in rocket engine turbopumps (Billonnet 1988) and in organic Rankine cycles (Bufi & Cinnella 2018). However, supersonic inlet turbines have to deal with the complexity of a diffusing stator: large stator outlet flow angles are prone to boundary layer separation, especially with oblique shock waves reflecting on the suction side; concurrently, flow separation may arise also on the rapidly extending endwalls. Further investigations are required to assess in detail benefits and disadvantages of operating in this area also for RDEs applications.

So far, zero incidence angle was considered at rotor inlet. If rotor geometry is conceived with a positive incidence angle, the maximum stator outlet flow angles allowed by the collective shock unstarting reduces. This consideration is relevant also for off-design operations and a designer should account for sufficient safety margins to avoid unstarting in design as well as in off-design.

Finally, it is of relevance to mention also stator-less configurations for RDEs (Paniagua et al. 2014). The design limits for this architecture are the same ones that were described for the rotor in a stator-rotor configuration, but the design process is easier from the limits point of view since it is free from the complex relation between stator outlet and rotor inlet limits.

CONCLUSIONS

The design of supersonic inlet turbines for rotating detonation engines is bounded by supersonic flows characteristic limits. This paper introduces a novel unstarting limit, which further constrains the design process of these machines. This additional unstarting mechanism is based on the generation of a collective shock from the coalescence of the leading-edge bow shock waves.

A procedure based on steady-state simulations was developed and validated to perform parametric analyses with limited computational cost. The parametric curves demonstrate that higher values of inlet geometric angles or incidence angles are more vulnerable to collective shock unstarting, while higher inlet Mach numbers improve safety margins. The shape of the bow shock waves and their intersection play a pivotal role in defining these trends.

An extensive overview of supersonic inlet turbine limits was provided, and the most severe limits were compared in function of relevant design parameters. Collective shock unstarting is the prevailing limit for almost all cases and neglecting this unstarting mechanism during the design stage may have critical consequences. Variable stator blade height is still a beneficial option to extend design limits and improve turbine efficiency, while the choice of the inlet Mach number is mainly driven by the required work specification.

REFERENCES

Anand, V. & Gutmark, E. (2019), 'Rotating detonation combustors and their similarities to rocket instabilities', *Progress in Energy and Combustion Science* **73**, 182–234.

Bach, E., Bohon, M. D., Paschereit, C. O. & Stathopoulos, P. (2019), Influence of nozzle guide vane orientation relative to RDC wave direction, *in* 'AIAA Propulsion and Energy Forum and Exposition, 2019'.

Billonnet, G. (1988), 'Flow Computation and Blade Cascade Design in Turbopump Turbines'.

Boiko, V. M., Klinkov, K. V. & Poplavskii, S. V. (2004), 'Collective Bow Shock Ahead of a Transverse System of Spheres in a Supersonic Flow Behind a Moving Shock Wave', *Fluid Dynamics* **39**(2), 330–338.

Braun, J., Paniagua, G. & Ferguson, D. (2021), Aero-Thermal Characterization of Accelerating and Diffusing Passages Downstream of Rotating Detonation Combustors, *in* 'ASME Turbo Expo 2021', pp. GT2021–59111.

Braun, J., Saracoglu, B. H. & Paniagua, G. (2017), 'Unsteady performance of rotating detonation engines with different exhaust nozzles', *Journal of Propulsion and Power* **33**(1), 121–130.

Bufi, E. A. & Cinnella, P. (2018), 'Preliminary Design Method for Dense-Gas Supersonic Axial Turbine Stages', *Journal of Engineering for Gas Turbines and Power* **140**(11).

Celik, I. B., Ghia, U., Roache, P. J., Freitas, C. J., Coleman, H. & Raad, P. E. (2008), 'Procedure for estimation and reporting of uncertainty due to discretization in CFD applications', *Journal of Fluids Engineering, Transactions of the ASME* **130**(7), 780011–780014.

Claflin, S., Sonwane, S., Lynch, E. & Stout, J. (2014), Recent advances in power cycles using rotating detonation engines with subcritical and supercritical CO2, *in* '4th International Symposium - Supercritical CO2 Power Cycles', Pittsburgh.

Coull, J. D. (2017), 'Endwall Loss in Turbine Cascades', *Journal of Turbomachinery* **139**(8).

Délery, J. & Dussauge, J. P. (2009), 'Some physical aspects of shock wave/boundary layer interactions', *Shock Waves* .

Druguet, M. C. & Zeitoun, D. E. (2003), 'Influence of numerical and viscous dissipation on shock wave reflections in supersonic steady flows', *Computers and Fluids* .

Frolov, S. M., Dubrovskii, A. V. & Ivanov, V. S. (2013), 'Three-dimensional numerical simulation of operation process in rotating detonation engine', *Progress in Propulsion Physics* **4**, 467–488.

Goldman, L. J. & Vanco, M. R. (1971), 'Computer Program for Design of Two-Dimensional Sharp-Edged-throat Supersonic Nozzle with Boundary-Layer Correction', *NASA* .

Jones, S. M. & Paxson, D. E. (2013), Potential Benefits to Commercial Propulsion Systems from Pressure Gain Combustion, *in* '49th AIAA/ASME/SAE/ASEE Joint Propulsion Conference', Joint Propulsion Conferences, American Institute of Aeronautics and Astronautics.

Kantrowitz, A. & Donaldson, C. (1945), 'Preliminary inversitagtion of supersonic diffusers', *NACA Wartime reports* .

Klapproth, J. F. (1950), Approximate relative-total-pressure losses of an infinite cascade of supersonic blades with finite leading-edge thickness, Technical report.

Knuth, D. E. (1997), *The art of computer programming*, Vol. 3, Pearson Education.

Laurence, S. J., Deiterding, R. & Hornung, G. (2007), 'Proximal bodies in hypersonic flow', *Journal of Fluid Mechanics* **590**, 209–237.

Liu, Z., Braun, J. & Paniagua, G. (2019), 'Characterization of a Supersonic Turbine Downstream of a Rotating Detonation Combustor', *Journal of Engineering for Gas Turbines and Power* **141**(3), 1–13.

Ma, J. Z., Luan, M.-Y., Xia, Z.-J., Wang, J.-P., Zhang, S.-j., Yao, S.-b. & Wang, B. (2020), 'Recent Progress, Development Trends, and Consideration of Continuous Detonation Engines', *AIAA Journal* **58**(12), 4976–5035.

Moeckel (1921), 'Approximate method for predicting form and location of detached shock waves ahead of plane or axially symmetric bodies', *NASA TN 1921* **211**(1), 130.

Moore, J. & Moore, J. G. (1983), 'Entropy Production Rates From Viscous Flow Calculations: Part I - A Turbulent Boundary Layer Flow'.

Mushtaq, N., Colella, G. & Gaetani, P. (2022), 'Design and Parametric Analysis of a Supersonic Turbine for Rotating Detonation Engine Applications', *International Journal of Turbomachinery, Propulsion and Power* **7**(1).

Mushtaq, N., Persico, G. & Gaetani, P. (2022), The Role of Endwall Shape Optimization in the Design of Supersonic Turbines for Rotating Detonation Engines, *in* 'ASME Turbo Expo 2022', pp. GT2022–82424.

Paniagua, G., Iorio, M. C., Vinha, N. & Sousa, J. (2014), 'Design and analysis of pioneering high supersonic axial turbines', *International Journal of Mechanical Sciences* **89**, 65–77.

Paxson, D. E. & Naples, A. (2017), 'Numerical and analytical assessment of a coupled rotating detonation engine and turbine experiment', *AIAA SciTech Forum - 55th AIAA Aerospace Sciences Meeting* (January), 1–14.

Prasad, A. (2004), 'Calculation of the Mixed-Out State in Turbomachine Flows', *Journal of Turbomachinery* **127**(3), 564–572.

Rankin, B. A., Fotia, M. L., Naples, A. G., Stevens, C. A., Hoke, J. L., Kaemming, T. A., Theuerkauf, S. W. & Schauer, F. R. (2017), 'Overview of performance, application, and analysis of rotating detonation engine technologies', *Journal of Propulsion and Power* **33**(1), 131–143.

Schwer, D. & Kailasanath, K. (2010), 'Numerical Investigation of Rotating Detonation Engines', (July).

Settles, G. S. & Dodson, L. J. (1991), Hypersonic shock/boundary-layer interaction database, *in* 'AIAA 22nd Fluid Dynamics, Plasma Dynamics and Lasers Conference, 1991'.

Shen, D., Cheng, M., Wu, K., Sheng, Z. & Wang, J. (2022), 'Effects of supersonic nozzle guide vanes on the performance and flow structures of a rotating detonation combustor', *Acta Astronautica* **193**, 90–99.

Sod, G. A. (1977), 'A numerical study of a converging cylindrical shock', *Journal of Fluid Mechanics* .

Sousa, J., Paniagua, G. & Collado Morata, E. (2017), 'Thermodynamic analysis of a gas turbine engine with a rotating detonation combustor', *Applied Energy* **195**, 247–256.

Sousa, J., Paniagua, G. & Saavedra, J. (2017), 'Aerodynamic response of internal passages to pulsating inlet supersonic conditions', *Computers and Fluids* **149**, 31–40.

Starken, H., Yongxing, Z. & Schreiber, H.-A. (1984), 'Mass Flow Limitation of Supersonic Blade Rows due to Leading Edge Blockage'.

Stewart, W. (1955), 'Analysis of two-dimensional compressible-flow loss characterisitics downstream of turbomachine blade rows in terms of basic boundary-layer characteristics', *NACA Technical Note 3515* .

Strakey, P., Ferguson, D., Sisler, A. & Nix, A. (2016), Computationally Quantifying Loss Mechanisms in a Rotating Detonation Engine, *in* '54th AIAA Aerospace Sciences Meeting', AIAA SciTech Forum, American Institute of Aeronautics and Astronautics.

Stratford, B. S. & Beavers, G. S. (1961), 'The Calculation of the Compressible Turbulent Boundary Layer in an Arbitrary Pressure Gradient - A Correlation of certain previous Methods', *Aeronautical Research Council Reports* (3207).

Wintenberger, E. & Shepherd, J. E. (2006), 'Thermodynamic Cycle Analysis for Propagating Detonations', *Journal of Propulsion and Power* **22**(3), 694–698.

Wolański, P. (2013), 'Detonative propulsion', *Proceedings of the Combustion Institute* **34**(1), 125–158.